# Simulation of Fault Detection in Photovoltaic System Based On SSTDR

Zhihua Li, Zhanfei Yang, Chunhua Wu
Shanghai Key Laboratory of power station, Department of Electrical Engineering, Shanghai University
Baoshan District, Shanghai 200444, China
e-mail: lzh_sh@staff.shu.edu.cn, yzfchifan@163.com, wuchunhua@shu.edu.cn

***Abstract*—Spread spectrum time domain reflectometry (SSTDR) is a broadband electrical reflectometry technique that has been successfully used to detect and locate faults on live electrical systems, including power systems, even photovoltaic (PV) systems. The high-frequency equivalent circuits of PV system, including DC bus cable, connecting wire and PV cell are analyzed in the paper. Detection simulations of ground faults, line-to-line faults and approximate open-circuit faults caused by aging in PV string are carried out and analyzed. The results of the simulation in Matlab indicate the effectiveness of SSTDR for different faults detection in photovoltaic array.**

***Keywords-SSTDR; ground faults; line-to-line faults; approximate open-circuit faults; PV fault detection***

## I. INTRODUCTION

With the continuous development of industry, the demand for energy is increasingly higher. The PV power is regarded as one of the most likely ways to replace fossil energy power generation in the future due to its abundant resources, safety, clean and easy installation. However, PV systems are often exposed in harsh outdoor environments to require sufficient sunlight, which will easily lead to aging problems in PV systems. Degraded PV modules and connecting wires can easily lead to faults in PV systems. According to statistics, the cost of photovoltaic array in photovoltaic power station can account for 40%-50% of the construction cost of the entire photovoltaic power station, so the failure of photovoltaic array often leads to the decline of output power of photovoltaic array, the damage of accelerating components, and even the fire. At the same time, ground faults, open-circuits fault and line-to-line faults are common electrical problems of photovoltaic array.

Traditional dc ground faults detection for grounded photovoltaic system is mainly by monitoring the currents changes, when current more than the threshold current, the electrical switch will interrupt circuit [1]. For the power loss and blind spot problems caused by fault detection, distributed capacitance can be used to monitor the voltage, so that neither power loss nor blind spot will be generated, and the reliability of detecting the photovoltaic system ground fault can be improved [2]. In ungrounded photovoltaic systems, residual current monitoring method [3] and dc insulation resistance measurement method [4] are commonly used to determine whether there is a grounding fault. For the line-to-line faults, traditional methods of detection and protection are still by connecting the over-current protection device (OCPDs) and photovoltaic group string series to monitor the changes of current. In addition, a fault detection and classification method based on decision trees (DT) [5] and the method of using three-layered artificial neural network to detect the line-to-line fault [6] also have good recognition effect. As for the open-circuit faults of photovoltaic modules, the most common detection method is to collect the output current and voltage signals of the photovoltaic system for analysis and fault diagnosis [7].

Although the above several photovoltaic string fault detection methods can detect faults, but they either need to install sensors for electrical information collection, or require a lot of calculation, or they cannot carry out online fault diagnosis. In this article, we evaluate the fault detection method based on Spread Spectrum Time Domain Reflectometry (SSTDR) for photovoltaic series, and verify the feasibility of detection for ground faults, line-to-line faults and open-circuit faults of photovoltaic series by simulation. A major advantage of this method over other reflectometry approaches is its ability to detect and locate faults within operating photovoltaic system.

## II. SSTDR DETECTION TECHNOLOGY SSTDR TECHNOLOGY

Reflectometry detection methods launch a small electrical signal on a wire and perform detailed analysis of the reflected signal to determine the location and severity of impedance discontinuities. SSTDR use a pseudo noise (PN) code or modulated PN code as their respective incident signals. The low magnitude of the PN code and its low interference with existing signals make it ideal candidate to be used on live electrical systems, such as PV panels. The block diagram of SSTDR detection system is shown in Fig.1. The PN sequences coming from generator modulated by the high-frequency sinusoidal carrier is injected into live electrical system, and it will reflect because of impedance discontinuities. The reflected signal returns to the SSTDR instrument, where it is cross-correlated with a delayed version of the incident signal to create the reflectometry response. The time correlation is given as (1).

Project Supported by National Natural Science Foundation of China (51677112).

978-1-7281-9026-6/20/$31.00 ©2020 IEEE

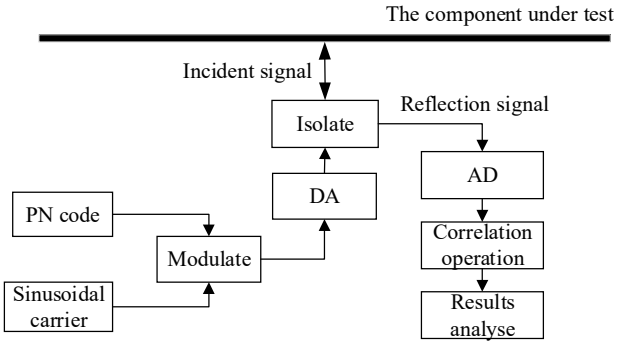


Figure 1. Block of fault detection with SSTDR.

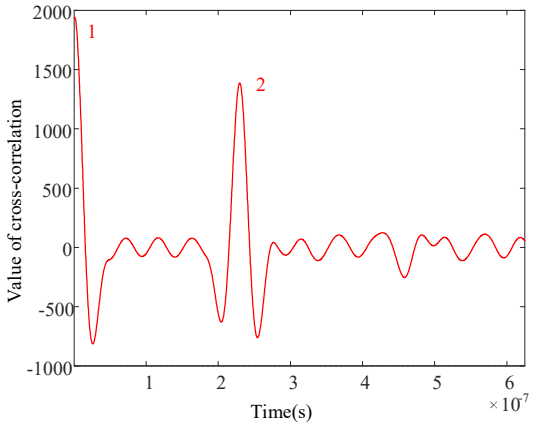


Figure 2. Measured SSTDR reflection responses for a live PV cable with open-circuit fault.

$$C(t)=\int_0^T s(t-\tau)s(t)dt \tag{1}$$

Where C(t) is the result of cross-correlation operation, s(t) is the incident signal, $s(t-\tau)$ is the reflected signal.

The reflectometry response of a live PV cable with open-circuit fault is shown in Figure 2. The magnitude and phase of the reflected signal are related to the type of impedance discontinuity, and the time delay between the incident signal and the various reflections indicate the distances to the discontinuities. In Figure 2, the time delay is the time between peak1 and peak2, while peak1 is caused by the impedance discontinuity at the incident point and peak2 is caused by impedance discontinuity by the fault in cable. The fault distance can be calculated according to equation (2).

$$dis=\frac{v_0\tau}{2} \tag{2}$$

Where $v_0$ is the speed of the incident signal in the cable, $\tau$ is the time delay.

## III. Equivalent Circuit Models of PV System

### A. PV DC Bus

The DC bus of PV system is a kind of parallel double conductor uniform transmission line, and its distributed parameter equivalent circuit is given in Figure 3, where $R_0$, $G_0$, $L_0$ and $C_0$ are the resistance, conductance, inductance and capacitance per unit length of the transmission line.

When The characteristic impedance Z is expressed as:

$$Z=\sqrt{\frac{R+j\omega L}{G+j\omega C}} \tag{3}$$

where R, G, L and C are the resistance, conductance, inductance and capacitance per unit length of the transmission line. If ωL≫R and ωC≫G at high frequency, the characteristic impedance can be reduced to $Z=\sqrt{L/C}$.

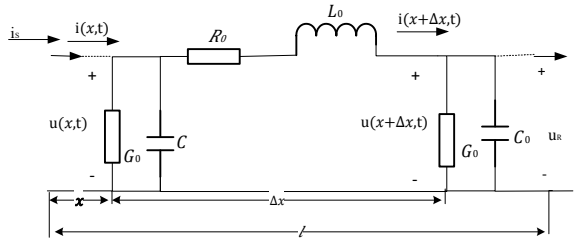


Figure 3. Distributied parameter model of uniform transmission line.

### B. Connecting wire between PV Modules

The connecting wire between PV modules is single-core wire. Its high-frequency approximate model is shown in Figure 4.

The ac resistance $R_{AC}$ and inductance $L_{ext}$ in Figure 4 are given as following:

$$\begin{cases} R_{AC}=\dfrac{r}{2\delta}R_{DC}=\dfrac{\sqrt{\pi\mu\sigma}}{2}R_{DC}\sqrt{f}=\dfrac{1}{2r}\sqrt{\dfrac{\mu}{\pi\sigma}}f \\ \delta=\dfrac{1}{\sqrt{\pi\mu\sigma f}} \end{cases} \tag{4}$$

$$L_{ext}=2\times10^{-7}l\left[\ln(2l/r)-1\right] \tag{5}$$

Where $R_{DC}=l/(\sigma\pi r^2)$, $l$ is the length of the wire, σ is conductivity, r is the radius of the wire; δ is the skin depth, $f$ is the operating frequency, μ is the permeability.

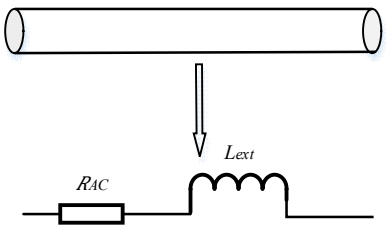


Figure 4. Equivalent lumped circuit model of connecting wire.

### C. Photovoltaic Cells

Individual PV cells have been modeled as a series/parallel combination of resistors, capacitors, and an inductor [8], which is shown in Figure 5. The photocurrent from illumination is introduced as an illumination-dependent current source, $I_{light}$, but it does not play a role in the reflectometry propagation model.

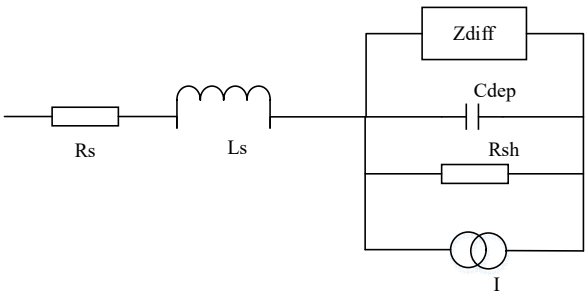


Figure 5. Photovoltaic cell equivalent lumped circuit model.

It can be found in [9] that the series resistance $R_s$ is determined by a host of individual resistance contributions: front busbars, front gridlines, interface between front contact metal and silicon, emitter sheet, bulk substrate, back metal, and back busbars. Under standard test condition, $R_s$ is about 1 Ω /cm$^2$[10]. The series inductance $L_s$ can be approximated by the inductance between two parallel and equal conductors. The value of $L_s$ is generally small, about $10^{-8}$ F/cm$^2$.

The shunt resistance $R_{sh}$ mainly accounts for the battery surface pollution and semiconductor crystal caused by the leakage current of the p-n junction leakage resistance and leakage resistance on the edge of the battery, the unit of $R_{sh}$ is in commonly KΩ. The depletion capacitance arises from the separation of charge densities across the depletion width. $C_{diff}$ is the dominant capacitance when the PV cell is under illumination, and $C_{dep}$ dominates when the PV cell is dark[2].

The expression of $Z_{diff}$ can be given by the differential complex impedance of the p-n junction diode [9]. When the complex impedance $Z_{diff}$ is positively biased, the injected current will cause a very large diffusion capacitor $C_{diff}$ and a large shunt conductance $G_{diff}$.

## IV. Simulation of Fault Detection Based on SSTDR

### A. Ground faults

Ground fault is a very common fault in PV systems, which will occur when there is a connection between a current-carrying conductor and a grounding path.

A schematic sketch of ground fault detection using SSTDR is given in Figure 6, where the dotted line shows the grounding plane. The value of grounding $R_g$ may vary from several ohms to several thousand ohms. The grounding current is smaller with higher impedance $R_g$. Ground faults with lower grounding impedance are more hazardous to PV system. Simulation of low impedance ground faults detection with SSTDR will be carried out in this paper.

The equivalent circuit model of a PV string with 4 modules shown in Figure 6 will be setup in Matlab/Simulink according to above analysis. The SSTDR signal is injected to the PV string through a 50m transmission- line. The parameters we use are follows: The frequency of SSTDR is 1.25e7 Hz, the L is 0.35e-3 H/km, the C is 0.14e-6F/km, so the characteristic impedance of the line is 50Ω. $R_s$ is 0.1Ω, $L_s$ is 1e-8H, $C_{diff}$ is ie-5F,$R_{diff}$ is 1e4Ω, $R_{sh}$ is 1e5Ω, $C_{dep}$ is 1e-4F [9][11].

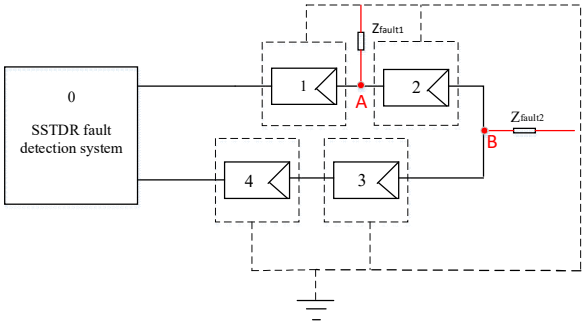


Figure 6. Schematic diagram of ground fault detection in a PV string.

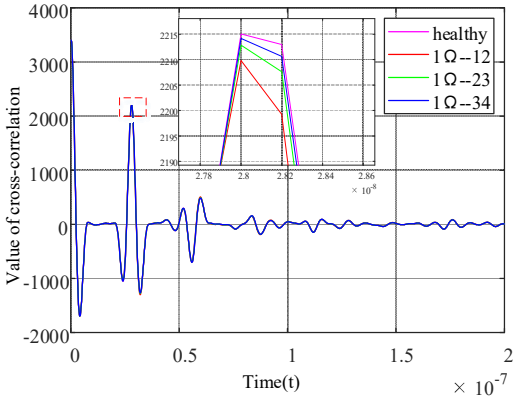


Figure 7. Simulation results of ground fault detection with $R_g$=1Ω.

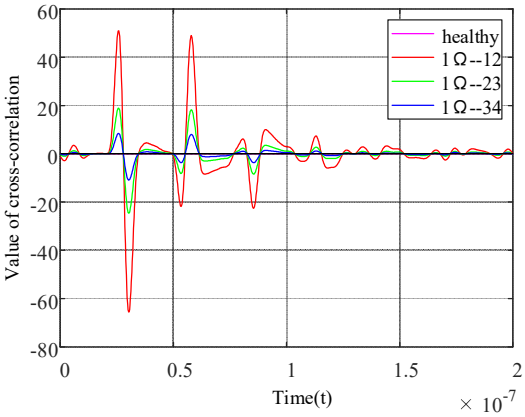


Figure 8. Processed results of ground faults detection.

When the grounding resistance $R_g$ is set to 1 Ω, the simulation detection results of different grounding position A, B, C are shown in Figure 7, where the waveform in the red rectangle is enlarged to be displayed more vivid. It can be found that with different grounding locations the amplitude of the peaks are different, where the peak of normal is the largest, and the peaks become smaller with the distance form the SSTDR test unit become longer. The peak differences are probably caused by signal attenuation transmitting in the PV string.

In order to display the difference more clearly, we get Figure 8 by subtracting the normal data from the grounding fault data. It is obvious that the farther the grounding location in the string from the SSTDR test unit is, the lower the amplitude of the peak of the fault is.

It can be seen that the peak of normal PV string is always the highest and the peak with grounding faults is lower than that of the normal. Ground faults can be detected with SSTDR based on this characteristic. But the grounding location cannot be deduced by equation (2) because the time delay nearly the same in the simulation. Ground fault location in PV string with SSTDR need further research.

### *B. Line-to-line (LL)faults*

LL-faults can occur inter the PV string or intra the strings because of damage or insulation breakdown. An inter string LL-fault detection schematic sketch is shown in Figure 9, where point A and B are connected for mistaken. If the fault impedance $R_{LL}$ is small, it may short the PV module 2 and lead to output power decline. Simulations with different LL-fault resistance $R_{LL}$ values as 1Ω, 10 Ω, 100 Ω, 500 Ω are carried out and the results are shown in Figure10 and Figure 11, where Figure 11 is the difference result of the fault wave subtracting the normal wave.

It can be found from Figure 10 and Figure 11 that the peak of inter-string LL-faults are always lower than the peak of the normal, and the peak with LL-faults decrease with the increase of $R_{LL}$. According to Fig. 8 and Fig. 11, it can be found that the processed simulation results waves of ground faults and inter-string LL-fault are different, and it can be convinced that different faults can be distinguished from the shape of detected waveforms.

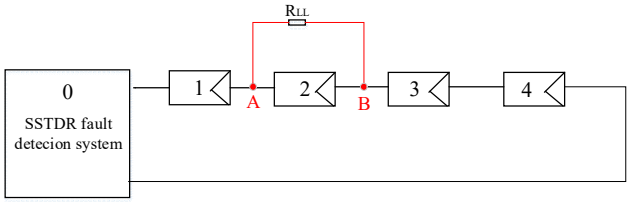


Figure 9. Schematic diagram of LL-fault detection.

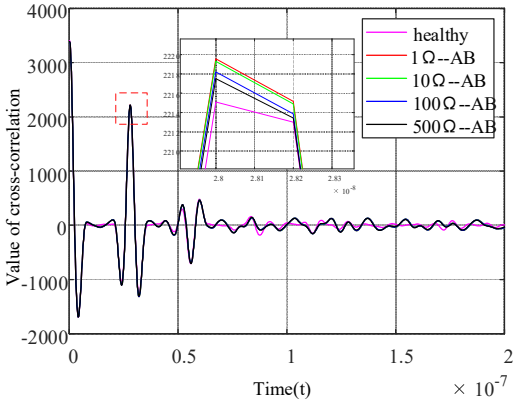


Figure 10. Simulation results of LL-faults detection with different $R_{LL}$

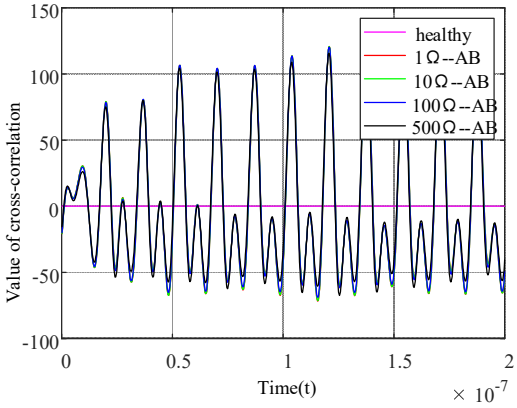


Figure 11. Processed results of LL-faults detection.

### *C. The deteriorating of PV string*

The outdoor severe environment deteriorates PV array gradually, which will lead to higher conducting resistances in PV modules, connecting terminals and wires. Aging in PV array will ultimately cause many kinds of faults such as open-circuit, arc and hot spots etc. It is very important to find out aging problems in PV array to keep PV system safe and effective.

Inserting a large series resistance to simulate the most severe deteriorating state in PV string, simulation detection of aging problems with SSTDR will be carried out. The schematic sketch is shown in Figure 12, where $R_D$ between module 1 and module 2 is the inserted series resistance.

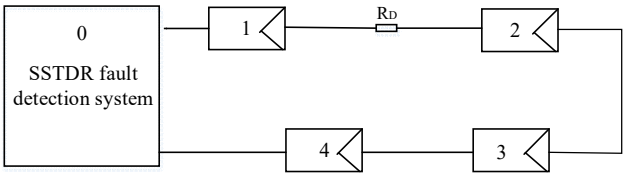


Figure 12. Schematic diagram of aging problem detection.

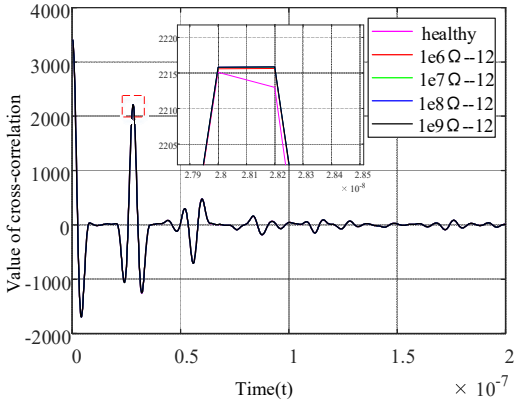


Figure 13. Simulation results of approximate open-circuit faults in PV string.

With the $R_D$ set to 10kΩ, 100kΩ, 1MΩ and 10MΩ respectively to simulate nearly open-circuit caused by aging

problem, the simulated waveforms are shown in Figure 13. The processed results with the same technique as above is shown in Figure 14.

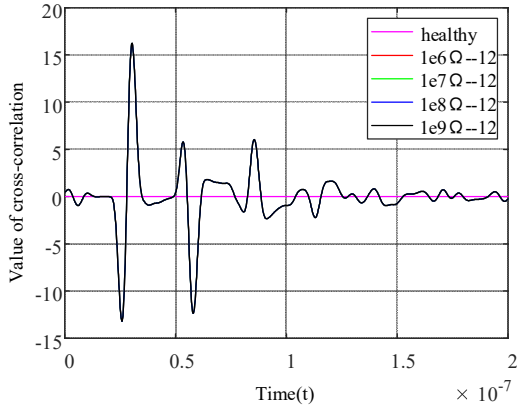


Figure 14. Processed results of approximate open-circuit faults detection.

From Figure13 and Figure 14, it can be found that the peaks with $R_D$ are lower than that of the normal, and the peak become higher when an approximate open circuit fault occurs in the photovoltaic module, the peak of the fault is bigger than the normal peak, and it increases as the fault impedance increases. Comparing Fig. 8, Fig. 11 and Fig. 14, we can clearly find the differences between the grounding fault, inter-string fault and approximate open circuit fault in the photovoltaic series.

## V. CONCLUSION

The PV string including PV cell, connecting wire and bus cable (transmission line) is modeled and detection simulations of ground faults, LL-faults and approximate open-circuit faults in PV string with SSTDR are carried out. The results show that there are differences in shapes and amplitudes of wave peaks obtained through SSTDR test with different faults condition. It is convinced that many kinds of faults in PV system can be detected based on SSTDR technique. But faults location in PV String with SSTDR need much more research to make it clear.

## REFERENCES


[1] S. Roy, M. K. Alam, F. Khan, J. Johnson and J. Flicker, "An Irradiance-Independent, Robust Ground-Fault Detection Scheme for PV Arrays Based on Spread Spectrum Time-Domain Reflectometry (SSTDR)," in IEEE Transactions on Power Electronics, vol. 33, no. 8, pp. 7046-7057, Aug. 2018, doi: 10.1109/TPEL.2017.2755592.

[2] Flicker J . Photovoltaic Ground Fault and Blind Spot Electrical Simulations[J]. office of scientific & technical information technical reports, 2013.

[3] M. K. Alam, F. Khan, J. Johnson and J. Flicker, "A Comprehensive Review of Catastrophic Faults in PV Arrays: Types, Detection, and Mitigation Techniques," in IEEE Journal of Photovoltaics, vol. 5, no. 3, pp. 982-997, May 2015.

[4] Flicker J , Johnson J . Photovoltaic ground fault detection recommendations for array safety and operation[J]. Solar Energy, 2016, 140(dec.15):34-50.

[5] Y. Zhao, L. Yang, B. Lehman, J. de Palma, J. Mosesian and R. Lyons, "Decision tree-based fault detection and classification in solar photovoltaic arrays," 2012 Twenty-Seventh Annual IEEE Applied Power Electronics Conference and Exposition (APEC), Orlando, FL, 2012, pp. 93-99.

[6] Syafaruddin, E. Karatepe and T. Hiyama, "Controlling of artificial neural network for fault diagnosis of photovoltaic array," 2011 16th International Conference on Intelligent System Applications to Power Systems, Hersonissos, 2011, pp. 1-6.

[7] Munoz M A , M.C. Alonso-García, Vela N , et al. Early degradation of silicon PV modules and guaranty conditions[J]. Solar Energy, 2011, 85(9):2264-2274.

[8] C. Furse, et al., "Spread Spectrum Time Domain Reflectometry for Complex Impedances: Application to PV Arrays," presented at the IEEE AutoTestCon, National Harbor, MD, 2018.

[9] M. U. Saleh et al., "Signal Propagation Through Piecewise Transmission Lines for Interpretation of Reflectometry in Photovoltaic Systems," in IEEE Journal of Photovoltaics, vol. 9, no. 2, pp. 506-512, March 2019, doi: 10.1109/JPHOTOV.2018.2884011.

[10] D. L. Meier et al., "Determining Components of Series Resistance from Measurements on a Finished Cell," 2006 IEEE 4th World Conference on Photovoltaic Energy Conference, Waikoloa, HI, 2006, pp. 1315-1318.

[11] T. Tanahashi, N. Sakamoto, H. Shibata and A. Masuda, "Electrical detection of gap formation underneath finger electrodes on c-Si PV cells exposed to acetic acid vapor under hygrothermal conditions," 2016 IEEE 43rd Photovoltaic Specialists Conference (PVSC), Portland, OR, 2016, pp. 1075-1079, doi: 10.1109/PVSC.2016.7749778.